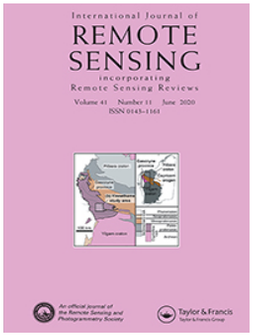

International Journal of Remote Sensing

ISSN: 0143-1161 (Print) 1366-5901 (Online) Journal homepage: https://www.tandfonline.com/loi/tres20

# Interannual variability and trends in sea surface temperature, sea surface wind, and sea level anomaly in the South China Sea

Chunli Liu, Xue Li, Sufen Wang, Danling Tang & Donghe Zhu

**To cite this article:** Chunli Liu, Xue Li, Sufen Wang, Danling Tang & Donghe Zhu (2020) Interannual variability and trends in sea surface temperature, sea surface wind, and sea level anomaly in the South China Sea, International Journal of Remote Sensing, 41:11, 4160-4173, DOI: 10.1080/01431161.2020.1714777

**To link to this article:** https://doi.org/10.1080/01431161.2020.1714777

Published online: 27 Jan 2020.

INTERNATIONAL JOURNAL OF REMOTE SENSING
2020, VOL. 41, NO. 11, 4160–4173
https://doi.org/10.1080/01431161.2020.1714777

Taylor & Francis
Taylor & Francis Group



# Interannual variability and trends in sea surface temperature, sea surface wind, and sea level anomaly in the South China Sea

Chunli Liu[a], Xue Li[b], Sufen Wang[c], Danling Tang[c] and Donghe Zhu[d]

[a]Marine College, Shandong University, Weihai, China; [b]State Key Laboratory of Marine Environmental Science, College of Ocean and Earth Sciences, Xiamen University, Xiamen, China; [c]State Key Laboratory of Tropical Oceanography, Guangdong Key Laboratory of Remote Sensing, South China Sea Institute of Oceanology, Chinese Academy of Sciences, Guangzhou, China; [d]Ocean College, Zhejiang University, Zhoushan, China

**ABSTRACT**

In this study, we analysed the interannual variability of sea surface temperature (SST), sea surface wind (SSW), and sea level anomaly (SLA) in the South China Sea (SCS) during 1985–2016 using monthly reanalysis and satellite datasets. An empirical orthogonal function (EOF) analysis was performed to evaluate the interannual variability of each variable. The warming rate of SST was 0.18 ± 0.26°C decade$^{-1}$ in the SCS. The first EOF of SST was characterized by basin-wide warming, with the highest anomalies in the northern deep basin. The first temporal coefficient of SST was negatively correlated with the Niño 3.4 index, with a lag of 6 mo. The mean rising rate of SLA was 7.6 cm decade$^{-1}$, with the greatest trend in the coastal water of Vietnam, which exhibited a similar spatial pattern with the first EOF of SLA. The temporal coefficient of SLA was negatively correlated with that of SST, with a lag of 5 mo. The trend of SSW was around 0.8 m s$^{-1}$ decade$^{-1}$ over the SCS. The first EOF of SSW was characterized by an anticyclonic pattern. The temporal coefficient was correlated with that of SST, with a lead of 2 mo. Wavelet coherence was used to investigate the cross-correlation relationship between SST and other variables. SST and SLA had a strong negative correlation in the 8–16-mo (1–1.5 yr) band. The high positive wavelet coherencies between SST and SSW and Niño 3.4 were mainly in the 32–64 mo (3–5 yr) band in the SCS.

**ARTICLE HISTORY**
Received 21 May 2019
Accepted 22 October 2019

## 1. Introduction

The South China Sea (SCS) is one of the largest marginal seas in the world. It extends from the Karimata Strait (~ 3°S) to the Taiwan Strait (23.5°N); it is bordered on the west by the Asian continent, Indo-China Peninsula, Malay Peninsula, and Borneo and on the east by Taiwan south to the Sulu Sea through the Mindoro Strait (Figure 1). The deep basin lies in the northern central part of the SCS, with a maximum depth of about 5000 m. In the northwest of the deep basin, a shelf extends about 250 km from the mainland coast.

The SCS is under the modulation of the East Asian monsoon. The SCS is dominated by the northeasterly monsoon in winter, and the wind direction reverses to be southwesterly

**CONTACT** Chunli Liu chunliliu@sdu.edu.cn Marine College, Shandong University, Weihai, China

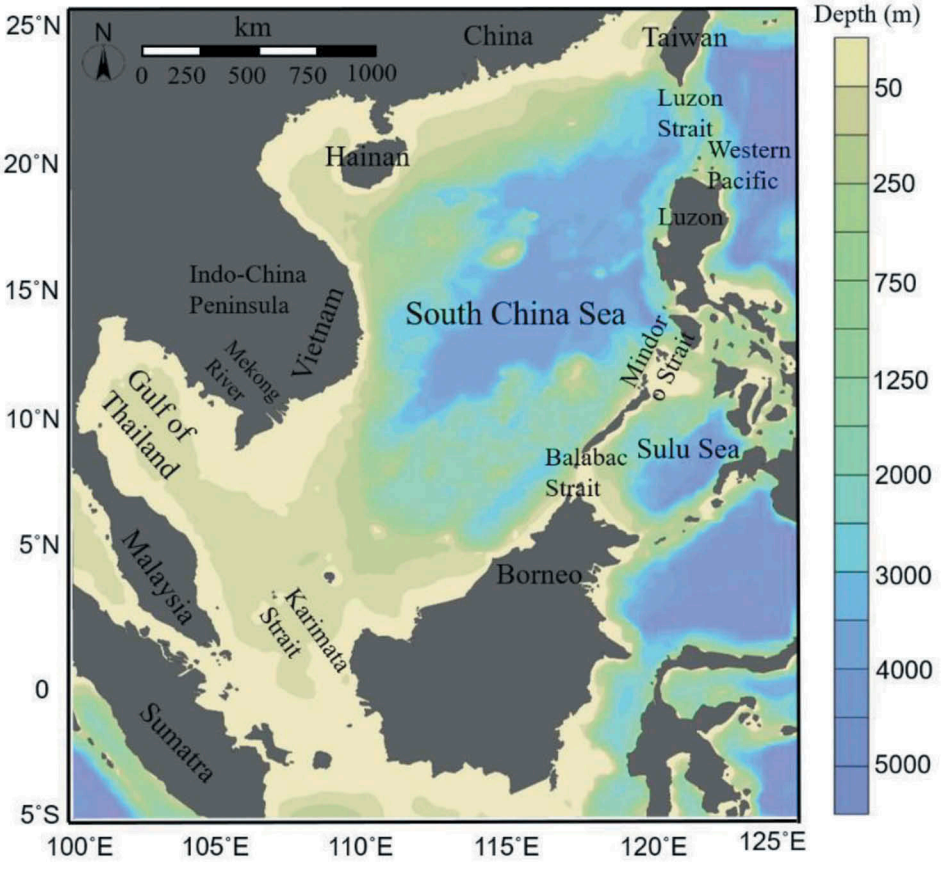


**Figure 1.** Map of the South China Sea (SCS).

in summer (Wyrtki 1961). In response to the northeasterly monsoon, the upper-ocean circulation is generally cyclonic. The summer circulation is characterized by an anticyclonic gyre in the southern basin and a weak cyclonic gyre in the north (Shaw and Chao 1994; Chu, Edmons, and Fan 1999; Shaw, Chao, and Fu 1999; Qu 2000). Correspondingly, sea surface temperature (SST), sea surface wind (SSW), and sea level anomaly (SLA) in the SCS display strong seasonal and interannual cycles. SST variation in the SCS can greatly influence extreme weather events and climate in the surrounding area on different time scales (Ding and Chan 2005; Wang, Ling, and Wang 2009; Ling et al. 2011; Kajikawa and Wang 2012; Liang et al. 2013; Xiang and Wang 2013; Vaid 2017). On the other hand, SST variation in the SCS influences SSW (Xie et al. 2003; Vaid and Polito 2016) and modulates the ocean's dynamic height (Shi et al. 2015). For instance, increased SST during the warm phase of El Niño-Southern Oscillation (ENSO) is often coupled with higher than average annual SLA in the eastern tropical Pacific.

There are many studies on the seasonal variability in SST, SSW, and SLA in the SCS (e.g., Chu, Lu, and Chen 1997; Ho et al. 2000a; Hwang and Chen 2000). Wang et al. (2002) reported a strong SCS warm event in 1997–1998, which was related closely to an ENSO event. Liu et al. (2004) found that the variability of the cold tongue in the SCS in winter was correlated

closely to Niño 3 and the SST anomaly. The anomalous SSW over the SCS was analysed by Chao, Shaw, and Wu (1996), especially for the 1982–1983 ENSO event. The analysis of Ho et al. (2000b) further revealed a response of the sea surface height in the SCS to an ENSO event. Li, Xu, and Cai (2002) found that the sea level in the SCS increased at a mean rate of 1 cm $yr^{-1}$ from 1993 to 1999. But studies mentioned above mostly focused on one particular variable or event using data of short temporal coverage. As a tropical marginal sea of the Pacific, the SCS exhibits remarkable interannual variability (Chu, Lu, and Chen 1997; Wen, Graf, and Huang 2000; Fang et al. 2006; Zhang et al. 2014). Therefore, with the availability of > 30 yr of the reanalysis product of SST and SSW, and > 20 years of satellite-observed SLA, we can now conduct an integrated analysis of these variables fields to provide a more systematic view of the trends and interannual variability in the SCS.

We aim to find the link between SST and other physical parameters in the SCS on an interannual time scale. Our objectives are as follows: 1) to identify the main modes of variability within every single reanalysis and satellite-derived dataset (SST, SLA, and SSW), 2) to study the trends of the three fields, and 3) to define the temporal correlation between SST and other fields.

## 2. Data and methods

Both monthly SST and SSW data were from the ERA-Interim dataset, a reanalysis product produced by the European Centre for Medium-Range Weather Forecasts (ECMWF) (Dee et al. 2011). SST and SSW data were collected during January 1985 – December 2016, which were on grids of 0.125° gird and 0.5° gird, respectively. The data covered the area from 3–24°N to 99–123°E in the western Pacific Ocean. Monthly SLA data used in the present work were from a 0.25° × 0.25° grid, which was produced by AVISO (archiving validation, and interpretation of satellite oceanographic data), France. SLA data were prepared by merging the TOPEX/Poseidon (TP), Jason-1, and ERS-1/2 altimeter observations. Because the SLA product began in September 1992, we only used data from January 1993 to December 2016.

The empirical orthogonal function (EOF) analysis is a statistical method that compresses the variability in a time-series of data with the aim of providing a compact description of their spatio-temporal variability of orthogonal functions (Lagerloef and Bernstein 1988; Baldacci et al. 2001; Navarro and Ruiz 2006; Parada and Canton 2010). The datasets of SST, SSW, and SLA were organized in a $(N \times M)$ matrix, where $N$ and $M$ represented the temporal and spatial elements, respectively. Because we focused on interannual variability in this study, seasonal cycles were first calculated by the annual-averaged original data from the monthly values of each dataset to obtain monthly anomalies. For the wavelet spectrum, the 12-mo running mean was one of the shortest filters to remove frequencies higher than one cycle per year (Emery and Thomson 2001). Thus, the amplitude modulation of the annual variation, or the interannual variability in seasonality, was also filtered out by the process. Alternatively, the spatial means of each pixel were removed. For example, the matrix $I(x,t)$ of SST can be written by$I(x,t) = \sum_{n=1}^{N} an(t)Fn(x)$, where $an(t)$ are the temporal evolution functions and $Fn(x)$ are the spatial eigen-functions for each mode.

## 3. Results and discussion

### 3.1. Seasonal cycle

First, we present the basic characteristics of the seasonal variability for mean fields of SST and SSW (32 yr) and mean fields of SLA (24 yr) during the study periods (Figure 2). The SST in summer is much more uniform than that in winter (Figure 2(a,d)). SLA demonstrated obvious negative values (dark blue) in the area off the southwest coast of the Mekong River Estuary (MRE) and off the east coast of Vietnam (Figure 2(b)), but it was yellow and green in most SCS areas. In addition, the southwesterly monsoon prevailed during summer, with the strongest wind speeds (> 7 m $s^{-1}$, Figure 2(c)) along the coastline of Vietnam between 7° and 13°N. In the northern SCS domain, water depth was > 1500 m, which was about 40 km away from the coastline and > 300 km from the MRE. Considering surface forcing and bathymetry, the favourable conditions for upwelling appeared locally (Figure 2(a), black arrow) off the east coast of Vietnam in summer. Colder water (< 29 °C) began near the coast and extended eastward towards the open sea.

In winter, SST was characterized by low values in the northwest basin and high values in the southeast basin (Figure 2(d)). The low temperature in the northwest was caused by the prevailing winter northeasterly wind (Figure 2(f)), which played an important role in

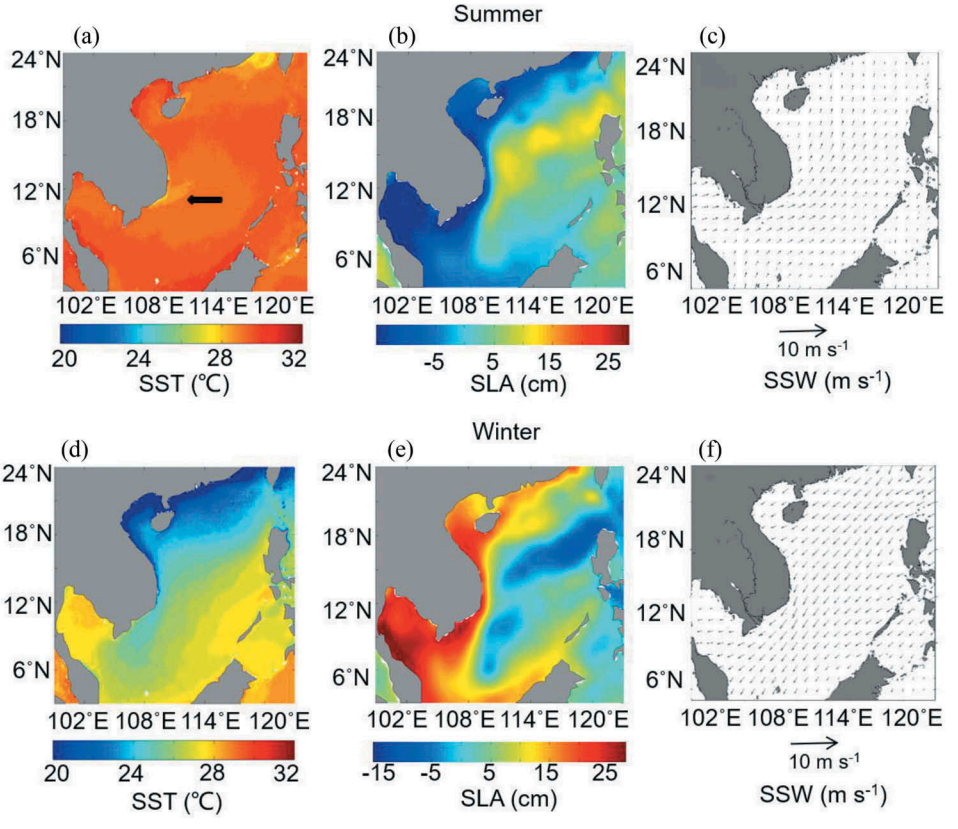


**Figure 2.** Summer- and winter-mean climatologies of sea surface temperature (SST), sea surface wind (SSW), and sea level anomaly (SLA) in the SCS.

cooling the SST in the northern SCS. First, winds brought cold and dry air to the SCS and, thus, cooled the surface through air-sea heat exchange. Second, wind generated a southwestward coastal current, which in turn brought cold coastal waters from the East China Sea and Taiwan Strait into the SCS (Chu, Edmons, and Fan 1999; Hu et al. 2000). In winter, the northeasterly wind had maximum wind speeds along the coastline of Vietnam between 8°N and 14°N, which was almost the same domain as that in summer, although it was stronger and broader than that in summer (> 9 m $s^{-1}$, Figure 2(c), winter). In this region, SLA in winter also opposite to that in summer (Figure 2(b)), which displayed- conditions favourable for downwelling (Gao et al. 2013). In addition, we observed low SLA in the southeast region and in the Luzon Strait of our study area in winter (Figure 2(f)), which was opposite to the high SLA in this region in summer.

### 3.2. Interannual variability

In the EOF decomposition, eigenvalues were ordered in terms of the percentage of variance they explained, which allowed a straightforward identification of the main modes of variability in the dataset; that is, the first eigenvalue explained higher amounts of the total variance. In this study, EOF analysis was performed for SST, SLA, and SSW after their respective climatological averages were removed first. Because the first three modes of SST, SLA, and SSW were all statistically significant, they were used further to explain the interannual variability in the SCS (Figures 3–5).

SST anomalies in the first EOF mode (54%) for the entire study area were all positive (Figure 3(a)), which indicated that the entire SCS exhibited basin-wide warming. The first temporal mode (Figure 3(d)) reached its peak in December-February and its valley in June-August, which responded to the cold northeasterly monsoon and the warm southwesterly monsoon, respectively. The temporal coefficient for this mode indicated high values during 1997–1998 and low values during 2011–2012. The spatial pattern (11% of the total variance, Figure 3(b)) of the second EOF mode exhibited distinct variation from the

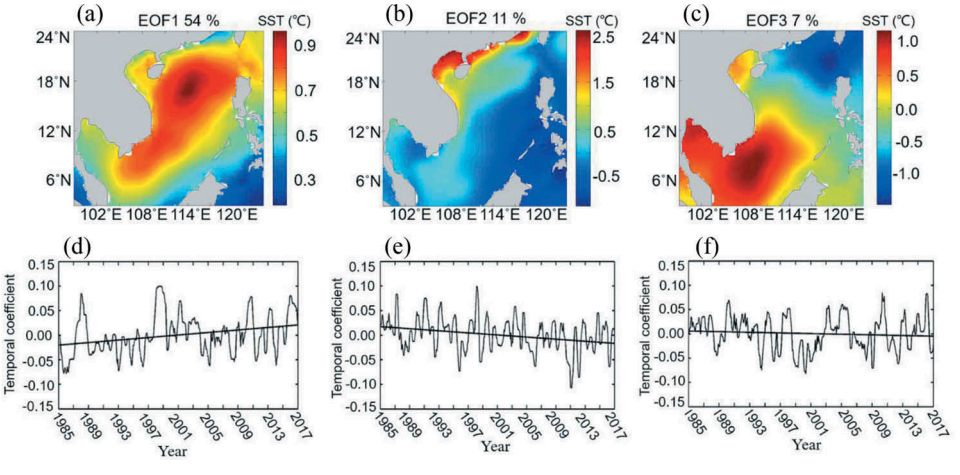


Figure 3. Spatial patterns and temporal coefficients of the first three empirical orthogonal function (EOF) modes of SST during the study period.

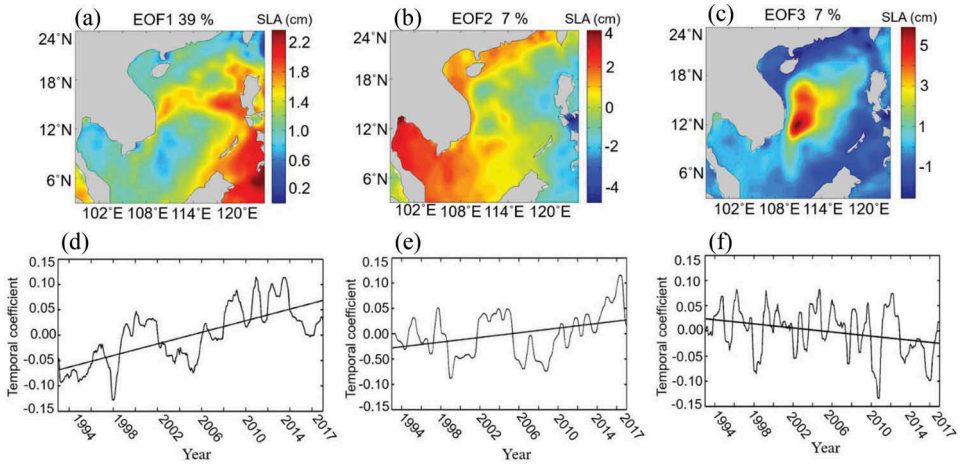


**Figure 4.** Spatial patterns and temporal coefficients of the first three EOF modes of SLA during the study period.

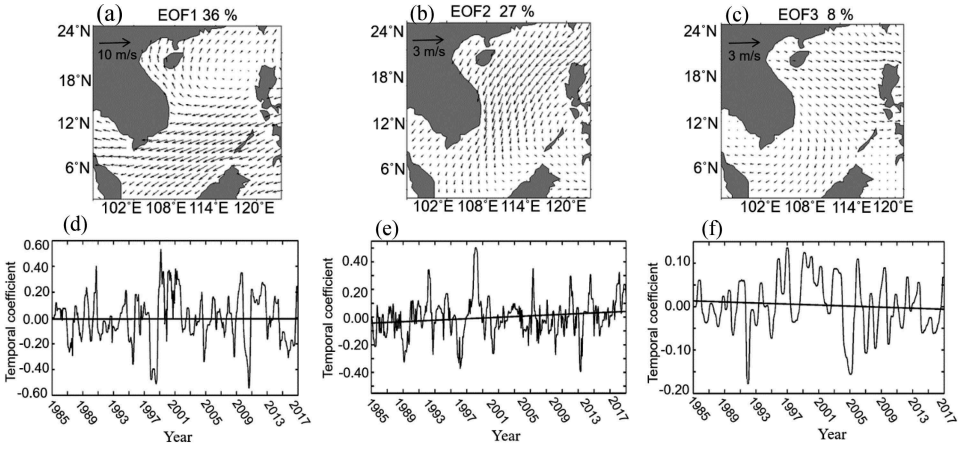


**Figure 5.** Spatial patterns and temporal coefficients of the first three EOF modes of SSW during the study period.

southeast (blue colour) to the northwest (green colour). This feature was not captured well in previous EOF analyses that demonstrated a strong north-to-south contrast across the SCS (Chu, Lu, and Chen 1997). The third EOF mode of SST demonstrated a dipole in the study area (7 % of the total variance, Figure 3(c)), with negative anomalies in the northeastern region and positive ones in the southwestern region.

The first EOF mode of SLA accounted for 39% of the total variance, which indicated that the entire basin experienced a rise in sea level during the study period (Figure 4(a)). However, the horizontal gradients in amplitude were large, and a major signal was apparent in the southeast part of the SCS. The second and third EOFs each accounted for 7% of the total variance. The second EOF mode of SLA demonstrated an opposite spatial pattern

compared with the first EOF mode (Figure 4(b)). The third EOF mode was due mainly to oscillations centred at 111°E, 12°N in the northern basin, which extended from Vietnam to Luzon; this revealed an upwelling signal in the study area (Figure 4(c)). The temporal coefficient of the first EOF mode demonstrated a rising trend with a rate of 0.06 cm $yr^{-1}$. It experienced a peak in December with negative values (< – 0.15) in 1998 (El Niño event), then large positive values persisted in 2011 (> 0.15) and 2012 (> 0.13) (Figure 4(d)). SLA that is driven by ENSO may be up 5–8 cm during strong El Niño/La Niña episodes (Tkalich et al. 2013). SST of the first EOF mode reached a peak and trough during 1998 and 2011, respectively, which indicated that SLA responded to SST variations throughout the water column (at least the upper 500–1000 m) (Cheng and Qi 2007). The temporal coefficient of the second EOF mode also demonstrated a slight rising trend (0.03 cm $yr^{-1}$) during the entire study period. The second EOF mode contributed positive anomalies to the remnant summer gyre in the southern basin and negative anomalies in the northern basin. For the third EOF mode, the summers of 1994, 1997, 2002, 2005, and 2012 favoured the formation of an eastward upwelling off Vietnam, which was consistent with the climatological summer feature shown in Zhao et al. (2018).

The first EOF of SSW (36%) demonstrated an anticyclonic pattern in the southern SCS. From this mode, the southeasterly monsoon (Figure 5(a)) intensified (weakened) during an ENSO warm (cold) phase over the entire southern SCS, but not in the northern SCS. The temporal coefficient of the first EOF mode indicated that the peaks (northeasterly monsoon) and valleys (southwesterly monsoon) often occurred in November-February and June-August, respectively (Figure 5(d)). Consequently, there was no distinct change in trend for the first EOF mode. The second EOF mode of SSW (Figure 5(b)) accounted for 27% of the total variance, which showed a cyclonic pattern. Note that the third EOF was characterized by spatial uniformity with an anticyclonic pattern, although the SSW speed showed no distinct difference. The temporal coefficients of the second and third EOF exhibited rising and dropping trends, although the rates were both small. The temporal coefficients for the three modes revealed interannual variability (Figure 5(d–f)). The anticyclone (cyclone) developed fully in the transition to the monsoon. From the spatial pattern of SSW EOF modes (Figure 5(a,b)), the anticyclone (cyclone) weakened the northeasterly (southwesterly) monsoon in the northern basin.

### 3.3. Spatial pattern

We calculated the trends in SST, SSW, and SLA over the SCS by fitting a linear function to each grid mesh after removing annual and semi-annual signals. The linear trend in SST showed a warming rate of 0.18 ± 0.26 °C $decade^{-1}$ during the period 1985–2016, which was less than both the estimated increases in SST in the SCS by 0.44 °C $decade^{-1}$ during 1982–2006 and 0.80 °C $decade^{-1}$ during 1957–2010 (Belkin 2009; Belkin 2016). The higher warming rates were in the northern deep basin, and lower rates appeared in the southern SCS (including the Sunda Shelf area) (Figure 6(a)). The highest rate exceeded 1 °C $decade^{-1}$ and was located west of the Taiwan Strait, where the SST warming rate was five times higher than that in the SCS. This is consistent with the variation in SST in the SCS in a previous study (Belkin and Lee 2014), which found that SST in the Taiwan Strait was three times higher than in the SCS. The warming trend became weaker towards the south. However, in the coastal waters over the northern region, we observed a cooling trend can

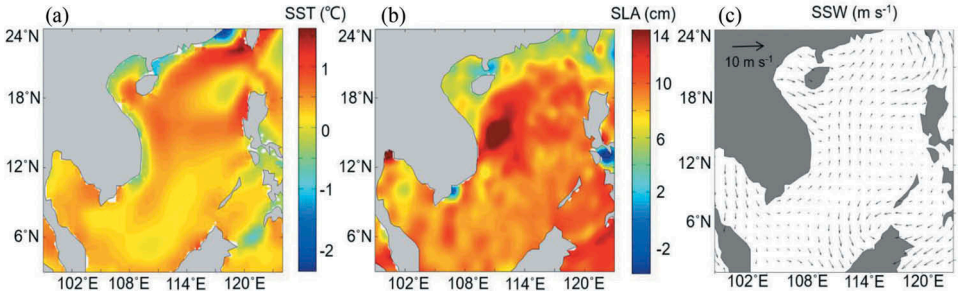


**Figure 6.** Trends in (a) SST, (b) SLA, and (c) SSW in the SCS during the study period.

be observed (Figure 6(a)). The warming rate of the SCS in the last 32 yr was greater than the global ocean mean warming rate (0.14 ± 0.04 °C decade$^{-1}$) between 1960 and 1990 (Casey and Cornillon 2001).

The SLA trend in the SCS was also not homogeneous. SLA showed rising trends in the range of 5–10 cm decade$^{-1}$ in most parts of the SCS (Figure 6(b)). The mean rate of increase in SLA was 7.6 cm decade$^{-1}$ for the SCS, which was about 3.0–3.7 times higher than the global mean SLA observed in the 1990s and during 1950–2000 (Cazenave and Nerem 2004; Church et al. 2004). However, the rate of increase in SLA in the present study was lower than that in Li, Xu, and Cai (2002), who estimated 1.0 cm yr$^{-1}$ for a shorter period (1993–1999). The greatest trend appeared along the east coast of Vietnam, which was influenced by the jet-shaped upwelling in this region. Moreover, the rate of increase in SLA in the southern Luzon Strait was higher than that in the northern strait, which indicated that the upper-layer westward transport in the Luzon Strait became weaker due to the westerly winds over the SCS (Figure 6(c)). The mean increasing trend in SSW of approximately 0.6 m s$^{-1}$ decade$^{-1}$ occurred over the SCS (Figure 6(c)). The westerly trend was consistent with a higher warming rate in the northern SCS than that in the southern SCS. A convergence of the SSW trend also occurred over the northern deep basin, which was also consistent with the greater increase in SST in this area.

### 3.4. Correlation between SST and oceanic parameters

SST in the SCS was influenced strongly by the East Asian monsoon. However, the drag of the wind on the sea surface moved the water in ways that not only changed SST, but also SLA (Pugh 2004). Therefore, we focused our analysis on the relationship of SST with SLA and SSW. Moreover, because SST variation in the SCS is also related closely to the ENSO on an interannual time scale (Qu et al. 2004; Wang et al. 2006), the influence of the ENSO on SST was also studied.

Figure 7(a,e) show that both SLA and Niño 3.4 were almost anti-phase with SSTA during the study period. The maximum correlation was – 0.42, with SSTA lagging Niño3.4 by 6 mo (Figure 7(f)) and with SSTA leading SLA by 5 months (Figure 7(b)), which agree with the results of Huynh et al. (2016). Moreover, the SSTA was positively correlated with SSW, with SSTA lagging SSW by 2 months (Figure 7(c,d)). The differences in the long-term estimates between the results obtained here and those by other authors (Fang et al. 2006; Liu et al. 2010; Soumya, Vethamony, and Tkalich 2015; Cheng et al. 2016) are were partly

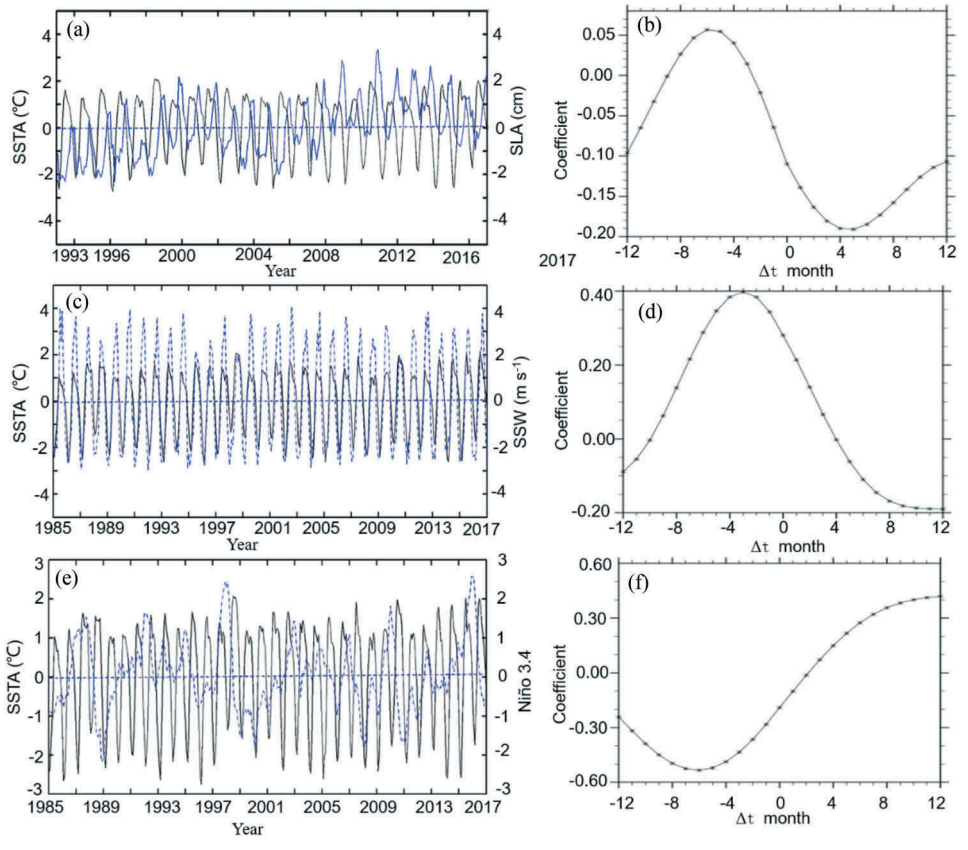


**Figure 7.** Left panels: (a) Time series of relationship between SST anomaly (SSTA) and SLA, (c) Time series of relationship between SSTA and SSW, and (e) Time series of relationship between SSTA and Niño 3.4. The black continuous lines are SSTA. The blue dot line is SLA (in Figure (a)), SSW (in Figure (c)) and Niño 3.4 (in Figure (e)), respectively. Right panels: (b) Cross-correlations between SSTA and SLA, (d) Cross-correlations between SSTA and SSW, and (f) Cross-correlations between SSTA and Niño 3.4.

due to differences in the length of the time-series and especially due to differences in the methods applied. The approach utilized here revealed that the long-term periodic components contributed considerably to the oceanographic data series. Also, it is worth noting that the length of the time series limited the extraction of natural oscillations. Consequently, time series should be long enough to extend over several cycles of natural variability modes to be extracted.

We also applied a wavelet coherence analysis (Grinsted, Moore, and Jevrejeva 2004) to SST with other oceanic variables (SLA, SSW, and Niño 3.4 index) in the SCS. Annual cycles and linear trends were removed from all the time series first to eliminate the influence of coherence with longer periods. The wavelet squared coherence values below the confidence level indicated more randomly distributed sections. The arrows in the images indicate the phase difference between SST and its counterpart at each time and period. The significant section showed a negative relationship between SST and SLA (Figure 8(a)), with arrows pointing left in the 8- to 16-mo (1–1.5 yr) band during 1993–2016. It was opposite for the wavelet coherency of SST and SSW (Figure 8(b)); the high positive

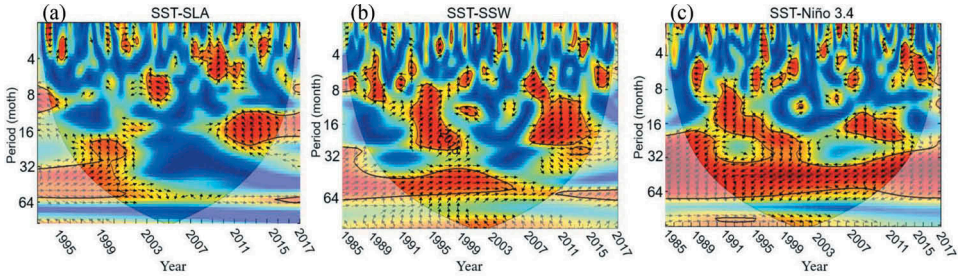


**Figure 8.** Wavelet coherency and phase between (a) SST and SLA, between (b) SST and SSW, and between (c) SST and Niño 3.4. Contours are squared wavelet coherencies that ranged from 0 to 1 (1 being the highest coherence). The thick black contour indicates the 5% significance level against red noise, and the lighter shade indicates the cone of influence, which represents possible edge effects. The relative phase relationship was shown as arrows with in-phase pointing to the right and anti-phase pointing to the left.

correlations were mainly in the 8- to 16- mo (1–1.5 yr) band. The high positive coherency occurred mainly in the 32- to 64- mo (3–5 yr) band in the entire study area for the wavelet coherency of SST and Niño 3.4 (Figure 8(c)), which was also observed for SLA and SSW during the study period.

## 4. Summary

The present study revealed interannual variability and trends in SST, SSW, and SLA in the SCS, using a long time series of the reanalysis and satellite-derived datasets. SST in the SCS was much more uniform in summer than in winter. The cold tongue off the east coast of Vietnam was an indication of upwelling in summer. In winter, SLA, not only along the east coast but also in the southeast region and the Luzon Strait, was opposite to the condition in summer. In addition, the southwesterly (northeasterly) monsoon prevailed in summer (winter) with the strongest wind speed that was almost in the same domain (coastline of Vietnam between 7° and 13°N). Wind speed was stronger and broader in winter (> 9 m $s^{-1}$) than in summer (> 7 m $s^{-1}$).

On the interannual time scale, the positive first EOF mode (54%) of SST indicated that the entire SCS exhibited basin-wide warming. The second and third EOF modes accounted for 11% and 7% of the total variance, respectively. The first EOF mode (39%) of SLA experienced a rise in sea level during the study period, and its temporal coefficient peaks in December were negative (< – 0.15) in 1998 and positive in 2011 (> 0.15) and 2012 (> 0.13). The first EOF mode of SSW (39%) demonstrated an anticyclonic pattern, and its temporal coefficient demonstrated significant interannual variability, with northeasterly monsoons and southwesterly monsoons that occurred in November-February and June-August, respectively. The three temporal coefficients all revealed interannual variability.

The mean rate of the SST trend was 0.18 ± 0.26 °C $decade^{-1}$ in the SCS, with higher warming rates in the northern deep basin and lower rates in the southern region. The mean rate of the SLA trend was 7.6 cm $decade^{-1}$, with the greatest trend in the coastal water of Vietnam that was influenced by the jet-shaped upwelling. The trend of SSW was

around 0.8 m $s^{-1}$ $decade^{-1}$ over the SCS. The westerly trend was consistent with a higher warming rate in the northern SCS than in the southern SCS.

SLA and Niño 3.4 were almost anti-phase with SSTA during the study period. The maximum correlation between SSTA and Niño 3.4 was – 0.42, with the SSTA lagging Niño 3.4 by 6 mo and with the SSTA leading the SLA by 5 mo. SSTA and SSW were positively correlated with SSTA that lagged SSW by 2 mo. These results could help to improve our understanding of ocean forcing factors that respond to climate change, and they could provide evidence for co-variability among them in the SCS. However, some fields in the ocean are still uncertain, and their response mechanisms to interannual variability to climate change need to be investigated in further studies.

## Disclosure statement

No potential conflict of interest was reported by the authors.

## Funding

This study was supported by the National Natural Science Foundation of China-Shandong joint fund [U1806203]; the National Science Foundation of China [41206166]; the Fundamental Research Funds for the Central Universities [2019ZRJC005]; the Postdoctoral Science Foundation of China [2017M622180]; the Foundation of Guangdong Key Laboratory of Ocean Remote Sensing (South China Sea Institute of Oceanology Chinese Academy of Sciences) [2017B030301005-LORS1803]; and the open fund of State Key Laboratory of Satellite Ocean Environment Dynamics, Second Institute of Oceanography [No.0702].

## References

Baldacci, A., G. Corsini, R. Grasso, G. Manzella, J. T. Allen, P. Cipollini, T. H. Guymer, and H. M. Snaith. 2001. "A Study of the Alboran Sea Mesoscale System by Means of Empirical Orthogonal Function Decomposition of Satellite Data." *Journal of Marine Systems* 29 (1–4): 293–311. doi:10.1016/S0924-7963(01)00021-5.

Belkin, I. M. 2009. "Rapid Warming of Large Marine Ecosystems." *Progress in Oceanography* 81 (1–4): 207–213. doi:10.1016/j.pocean.2009.04.011.

Belkin, I. M. 2016. "Sea Surface Temperature Trends in Large Marine Ecosystems." In *IOC-UNESCO and UNEP (2016). Large Marine Ecosystems: Status and Trends*, 101–109. Nairobi: United Nations Environment Programme.

Belkin, I. M., and M. A. Lee. 2014. "Long-term Variability of Sea Surface Temperature in Taiwan Strait." *Climatic Change* 124 (4): 821–834. doi:10.1007/s10584-014-1121-4.

Casey, K. S., and P. Cornillon. 2001. "Global and Regional Sea Surface Temperature Trends." *Journal of Climate* 14 (18): 3801–3818. doi:10.1175/1520-0442(2001)014<3801:garsst>2.0.co;2.

Cazenave, A., and R. S. Nerem. 2004. "Present-day Sea Level Change: Observations and Causes." *Reviews of Geophysics* 42 (3): RG3001. doi:10.1029/2003RG000139.

Chao, S. Y., P. T. Shaw, and S. Y. Wu. 1996. "El Niño Modulation of the South China Sea Circulation." *Progress in Oceanography* 38 (1): 51–93. doi:10.1016/S0079-6611(96)00010-9.

Cheng, X., S. P. Xie, Y. Du, J. Wang, X. Chen, and J. Wang. 2016. "Interannual-to-decadal Variability and Trends of Sea Level in the South China Sea." *Climate Dynamics* 46 (9–10): 3113–3126. doi:10.1007/s00382-015-2756-1.

Cheng, X. H., and Y. Q. Qi. 2007. "Trends of Sea Level Variations in the South China Sea from Merged Altimetry Data." *Global and Planetary Change* 57 (3–4): 371–382. doi:10.1016/j.gloplacha.2007.01.005.

Chu, P. C., N. L. Edmons, and C. W. Fan. 1999. "Dynamical Mechanisms for the South China Sea." *Deep-Sea Research Part I* 43 (4): 445–466. doi:10.1175/1520-0485(1999)029<2971:DMFTSC>2.0.CO;2.

Chu, P. C., S. Lu, and Y. Chen. 1997. "Temporal and Spatial Variabilities of the South China Sea Surface Temperature Anomaly." *Journal of Geophysical Research: Oceans* 102 (C9): 20937–20955. doi:10.1029/97jc00982.

Church, J. A., N. J. White, R. Coleman, K. Lambeck, and J. X. Mitrovica. 2004. "Estimates of the Regional Distribution of Sea Level Rise over the 1950–2000 Period." *Journal of Climate* 17 (13): 2609–2625. doi:10.1175/1520-0442(2004)017<2609:eotrdo>2.0.co;2.

Dee, D. P., S. M. Uppala, A. J. Simmons, P. Berrisford, P. Poli, S. Kobayashi, U. Andrae, et al. 2011. "The ERA-Interim Reanalysis: Configuration and Performance of the Data Assimilation System." *Quarterly Journal of the Royal Meteorological Society* 137 (656): 553–597. doi:10.1002/qj.828.

Ding, Y., and J. C. L. Chan. 2005. "The East Asian Summer Monsoon: An Overview." *Meteorology and Atmospheric Physics* 89 (1–4): 117–142. doi:10.1007/s00703-005-0125-z.

Emery, W. J., and R. E. Thomson. 2001. *Data Analysis Methods in Physical Oceanography*. 2nd ed, 638. New York: Elsevier. doi:10.2307/1353059.

Fang, G., H. Chen, Z. Wei, Y. Wang, X. Wang, and C. Li. 2006. "Trends and Interannual Variability of the South China Sea Surface Winds, Surface Height, and Surface Temperature in the Recent Decade." *Journal of Geophysical Research* 111: (C11) S16. doi:10.1029/2005JC003276.

Gao, S., H. Wang, G. Liu, and H. Li. 2013. "Spatio-temporal Variability of Chlorophyll a and Its Responses to Sea Surface Temperature, Winds and Height Anomaly in the Western South China Sea." *Acta Oceanologica Sinica* 32 (1): 48–58. doi:10.1007/s13131-013-0266-8.

Grinsted, A., J. C. Moore, and S. Jevrejeva. 2004. "Application of the Cross Wavelet Transform and Wavelet Coherence to Geophysical Time Series." *Nonlinear Processes in Geophysics* 11 (5/6): 561–566. doi:10.5194/npg-11-561-2004.

Ho, C., N. Kuo, Q. Zheng, and Y. S. Soong. 2000a. "Dynamically Active Areas in the South China Sea Detected from TOPEX/Poseidon Satellite Altimeter Data." *Remote Sensing of Environment* 71 (3): 320–328. doi:10.1016/s0034-4257(99)00094-2.

Ho, C. R., Q. Zheng, Y. S. Soong, N. J. Kuo, and J. H. Hu. 2000b. "Seasonal Variability of Sea Surface Height in the South China Sea Observed with TOPEX/Poseidon Altimeter Data." *Journal of Geophysical Research* 105 (C6): 13981–13990. doi:10.1029/2000JC900001.

Hu, J. Y., H. Kawamura, H. S. Hong, and Y. Q. Qi. 2000. "A Review on the Currents in the South China Sea: Seasonal Circulation, South China Sea Warm Current and Kuroshio Intrusion." *Journal of Oceanography* 56 (6): 607–624. doi:10.1023/a:1011117531252.

Huynh, H. N. T., A. Alvera-Azcárate, A. Barth, and J. M. Beckers. 2016. "Reconstruction and Analysis of Long-term Satellite-derived Sea Surface Temperature for the South China Sea." *Journal of Oceanography* 72 (5): 707–726. doi:10.1007/s10872-016-0365-1.

Hwang, C., and S. A. Chen. 2000. "Circulation and Eddies over the South China Sea Derived from TOPEX/Poseidon Altimetry." *Journal of Geophysical Research* 105 (C10): 23943–23965. doi:10.1029/2000JC900092.

Kajikawa, Y., and B. Wang. 2012. "Interdecadal Change of the South China Sea Summer Monsoon Onset." *Journal of Climate* 25 (9): 3207–3218. doi:10.1175/jcli-d-11-00207.1.

Lagerloef, G. S. E., and R. L. Bernstein. 1988. "Empirical Orthogonal Function Analysis of Advanced Very High Resolution Radiometer Surface Temperature Pattern in Santa Barbara Channel." *Journal of Geophysical Research* 93: (C6):6863–6873. doi:10.1029/jc093ic06p06863.

Li, L., J. Xu, and R. Cai. 2002. "Trends of Sea Level Rise in the South China Sea during the 1990s: An Altimetry Result." *Chinese Science Bulletin* 47 (7): 582–585. doi:10.1360/02tb9134.

Liang, J., Z. Wen, J. Chen, and L. Wu. 2013. "Characteristics of Tropical Sea Surface Temperature Anomalies and Their Influences on the Onset of South China Sea Summer Monsoon." *Atmospheric and Oceanic Science Letters* 6 (5): 266–272. doi:10.3878/j.issn.1674-2834.13.0026.

Ling, Z., G. Wang, C. Wang, and Z. Fan. 2011. "Different Effects of Tropical Cyclones Generated in the South China Sea and the Northwest Pacific on the Summer South China Sea Circulation." *Journal of Oceanography* 67 (3): 347–355. doi:10.1007/s10872-011-0044-1.

Liu, Q., X. Jiang, S. P. Xie, and W. T. Liu. 2004. "A Gap in the Indo-Pacific Warm Pool over the South China Sea in Boreal Winter: Seasonal Development and Interannual Variability." *Journal of Geophysical Research* 109 (C7): C07012. doi:10.1029/2003JC002179.

Liu, X., Y. Liu, L. Guo, Z. Rong, Y. Gu, and Y. Liu. 2010. "Interannual Changes of Sea Level in the Two Regions of the East China Sea and Different Responses to ENSO." *Global and Planetary Change* 72 (3): 215–226. doi:10.1016/j.gloplacha.2010.04.009.

Navarro, G., and J. Ruiz. 2006. "Elements of Spatial and Temporal Variability of Plankton in the Gulf of Cadiz: An Analysis Based on EOF Decomposition of SeaWiFS Images." *Proceedings of SPIE* 5233: 34–42. doi:10.1117/12.514031.

Parada, M., and M. Canton. 2010. "Sea Surface Temperature Variability in Alboran Sea from Satellite Data." *International Journal of Remote Sensing* 19 (13): 2439–2450. doi:10.1080/014311698214541.

Pugh, D. T. 2004. "Changing Sea Levels: Effects of Tides, Weather and Climate." *Cambridge University Press* 265 (pp). doi:10.1007/1-4020-3880-1_66.

Qu, T. 2000. "Upper-layer Circulation in the South China Sea." *Journal of Physical Oceanography* 30 (6): 1450–1460. doi:10.1175/1520-0485(2000)030<1450:ulcits>2.0.co;2.

Qu, T., Y. Y. Kim, M. Yaremchuk, T. Tozuka, A. Ishida, and T. Yamagata. 2004. "Can Luzon Strait Transport Play a Role in Conveying the Impact of ENSO to the South China Sea?" *Journal of Climate* 17 (18): 3644–3657. doi:10.1175/1520-0442(2004)0172.0.CO;2.

Shaw, P. T., and S. Y. Chao. 1994. "Surface Circulation in the South China Sea." *Deep-Sea Research Part I* 40 (11–12): 1663–1683. doi:10.1016/0967-0637(94)90067-1.

Shaw, P. T., S. Y. Chao, and L. L. Fu. 1999. "Sea Surface Height Variations in the South China Sea from Satellite Altimetry." *Oceanologica Acta* 22 (1): 1–17. doi:10.1016/S0399-1784(99)80028-0.

Shi, R., X. Y. Guo, D. X. Wang, L. L. Zeng, and J. Chen. 2015. "Seasonal Variability in Coastal Fronts and Its Influence on Sea Surface Wind in the Northern South China Sea." *Deep-Sea Research II* 119: 30–39. doi:10.1016/j.dsr2.2013.12.018.

Soumya, M., P. Vethamony, and P. Tkalich. 2015. "Inter-annual Sea Level Variability in the Southern South China Sea." *Global and Planetary Change* 133: 17–26. doi:10.1016/j.gloplacha.2015.07.003.

Tkalich, P., P. Vethamony, L.-Q. Hung, and M. Babu. 2013. "Sea Level Trend and Variability in the Singapore Strait." *Ocean Science* 9 (2): 293–300. doi:10.5194/os-9-293-2013.

Vaid, B. H. 2017. "Biweekly Sea Surface Temperature over the South China Sea and Its Association with the Western North Pacific Summer Monsoon." *Pure and Applied Geophysics* 174: 463–475. doi:10.1007/s00024-015-1198-3.

Vaid, B. H., and P. S. Polito. 2016. "Influence of the South China Sea Biweekly Sea Surface Temperature on the South China Sea Summer Monsoon Especially during the Indian Ocean Dipole." *Atmosphere-Ocean* 54 (1): 48–59. doi:10.1080/07055900.2015.1130682.

Wang, D., Q. Xie, Y. Du, W. Wang, and J. Chen. 2002. "The 1997–1998 Warm Event in the South China Sea." *Chinese Science Bulletin* 47 (14): 1221–1227. doi:10.1007/BF02907614.

Wang, G., Z. Ling, and C. Wang. 2009. "Influence of Tropical Cyclones on Seasonal Ocean Circulation in the South China Sea." *Journal of Physical Oceanography* 114 (C10): 022. doi:10.1029/2009JC005302.

Wang, Y., G. Fang, Z. Wei, F. Qiao, and H. Chen. 2006. "Interannual Variation of the South China Sea Circulation and Its Relation to El Niño, as Seen from a Variable Grid Global Ocean Model." *Journal of Physical Oceanography* 111: C11. doi:10.1029/2005JC003269.

Wen, C., H. F. Graf, and R. H. Huang. 2000. "The Interannual Variability of East Asian Winter Monsoon and Its Relation to the Summer Monsoon." *Advances in Atmospheric Sciences* 17 (1): 48–60. doi:10.1007/s00376-000-0042-5.

Wyrtki, K. 1961. "Physical Oceanography of the Southeast Asia Waters." *NAGA Report* 2: 1–195.

Xiang, B., and B. Wang. 2013. "Mechanisms for the Advanced Asian Summer Monsoon Onset since the Mid-to-late 1990s." *Journal of Climate* 26 (6): 1993–2009. doi:10.1175/JCLI-D-12-00445.1.

Xie, S., Q. Xie, D. Wang, and W. T. Liu. 2003. "Summer Upwelling in the South China Sea and Its Role in Regional Climate Variations." *Journal of Physical Oceanography* 108 (C8): 3261. doi:10.1029/2003jc001867.

Zhang, G. S., Q. Xu, Z. Gong, Y. C. Cheng, L. Wang, and Q. Y. Ji. 2014. "Annual and Interannual Variability of Scatterometer Ocean Surface Wind over the South China Sea." *Journal of Ocean University of China* 13 (2): 191–197. doi:10.1007/s11802-014-1993-y.

Zhao, H., J. Zhao, X. Sun, F. Chen, and G. Han. 2018. "A Strong Summer Phytoplankton Bloom Southeast of Vietnam in 2007, A Transitional Year from El Niño to La Niña." *PLoS One* 13 (1): e0189926. doi:10.1371/journal.pone.0189926.